Unraveling the Role of Low Coordination Sites in a Cu Metal Nanoparticle: A Step toward the Selective Synthesis of Second Generation Biofuels

Nicola Scotti,[†,§] Milind Dangate,[†,§] Antonella Gervasini,[‡] Claudio Evangelisti,[†] Nicoletta Ravasio,*[,†] and Federica Zaccheria[†]

[†]CNR, Institute of Molecular Science and Technologies (CNR-ISTM) and [‡]Dipartimento di Chimica, Università di Milano, Via Golgi 19, 20133 Milano, Italy

Ⓢ Supporting Information

ABSTRACT: The acidity of a prereduced Cu/SiO_2 catalyst was extensively investigated by means of FT-IR of adsorbed pyridine and by titration with 2-phenylethylamine in cyclohexane. Comparison with the parent CuO/SiO_2 material, which was already shown to exhibit Lewis acid sites due to the high dispersion of the CuO phase, provided evidence that reduction of this phase to the metallic state increases the acidity of the material. This allowed us to set up a bifunctional catalyst showing acidic and hydrogenation activity, both ascribable to the presence of the metal particle, without the need of an acidic support. This catalyst was tested in the one-pot transformation of γ—valerolactone into pentyl valerate and showed comparable activity (91% vs 92% conversion) and improved selectivity (92% vs 72%) with respect to the previously reported copper catalyst supported on acidic material. The role of Cu in activating the substrate was also evidenced through FTIR of adsorbed γ-valerolactone.

KEYWORDS: GVL, pentyl valerate, valeric fuels, supported Cu catalysts, solid Lewis acids
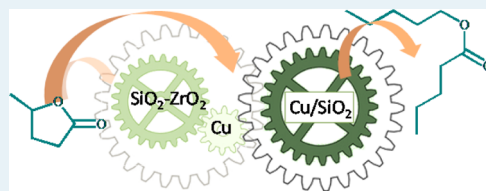
INTRODUCTION

In the search for renewable energy, we have several potential sources at hand: water, sunlight, wind, geothermal heat, and tidal flow can all be used to generate power. On the contrary, the search for renewable transportation fuels has to rely on only one source: biomass.

Among the different raw materials available from biomass, vegetable oils are very suitable for the synthesis of diesel components such as fatty acids methyl esters (biodiesel) and hydrocarbons obtained through hydrocracking of vegetable oils and fats (green diesel or renewable diesel),[1] but the most abundant biomass is cellulose, and for this reason its transformation in platform molecules has received increased attention in the past decade. These platform molecules were first pinpointed by the U.S. Department of Energy in 2004 in a report identifying 15 compounds as those having high potential for application in future biorefineries, which was revised in 2010 to include more recent advances in biomass conversion technologies.[2] Among the compounds listed in the 2010 review, levulinic acid can be considered one of the most important due to its reactive nature. Moreover, it can be produced from lignocellulosic wastes at low cost, for example, through the Biofine process that can be fed with agricultural residues, papermill sludge, or urban waste paper.[3]

Levulinic acid or its esters can be hydrogenated to furan derivatives[4,5] or to γ-valerolactone (GVL)[6–14] that in turn has been identified as a platform molecule with many applications as a precursor for chemicals,[15] as solvent,[16–18] fuel additive,[15] and fuels precursor.[19–25] Among the molecules that can be

obtained from GVL, valeric esters showed excellent features as gasoline or diesel fuel depending on the alcoholic residue.[26]

Some of us recently reported a process for the production of ethyl and pentyl valerate directly from GVL and the proper alcohol by using an heterogeneous copper catalyst supported on silica-zirconia.[27] The reaction with ethanol allowed us to elucidate the reaction mechanism and to test the stability and reusability of the catalyst, whereas using pentanol, GVL conversions higher than 90% and selectivities to pentyl valerate up to 83% were achieved. The reaction takes place under H_2 through nucleophilic addition of the alcohol to the carboxylic group giving hydroxypentanoate **1**, followed by dehydration to pentenoate **2** and hydrogenation to pentyl valerate **3** (Scheme 1).
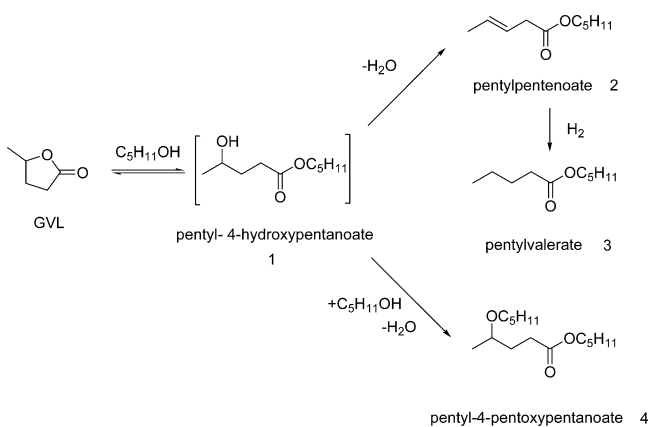
The acid-catalyzed reactions were ascribed to the acidic support, whereas hydrogenation activity was linked to the presence of supported copper.

However, it is well-recognized that the type and strength of acidic sites are very important in designing solid acid catalysts for renewable raw material transformations,[28,29] solid Lewis acids emerging as a very valuable alternative to Brønsted ones such as zeolites and sulfonated materials. The role of both the support and the catalyst acidity in the particular case of levulinic acid transformation to pentenoic acids or to valeric esters in the

Scheme 1. Reaction Mechanism for the Conversion of GVL into Pentyl Valerate

and dilution with highly deionized water (Milli-Q Academic, Millipore) to a final weight of 100 g.

2.2.2. N₂ Physisorption Measurements. Values of the sample surface area and porosity were determined (Table 1) by collecting N_2 adsorption/desorption isotherms at −196 °C using a Sorptomatic 1900 series instrument purchased from CE Instruments Ltd. Prior to the analysis, the sample (ca. 0.1 g) was outgassed at 150 °C for 2 h. Specific surface area was calculated by the BET equation in the relative pressure interval of $P/P_0 = 0.033-0.35$, assuming the N_2 molecular area in the adsorbed state as 16.2 Å². The total pore volume (cm³·g⁻¹, STP) was estimated from the total uptake of N_2 adsorbed at a relative pressure $P/P_0 = 0.99$, converted into liquid volume (cm³·g⁻¹) using the N_2 density in the normal liquid state ($\rho = 0.8081$ g cm⁻³). Pore size distribution was obtained from the desorption branch of the collected isotherm using the Barrett−Joyner−Halenda (BJH)[37] model equation.

2.2.3. Scanning Electron Micrographs. Scanning electron micrographs (SEM) were obtained by a JEOL JSM-5500LV coupled with energy dispersive X-ray spectroscopic (EDS) analyzer working at 20 keV to obtain quantitative information on the distribution of Cu and Si elements. The samples were analyzed under moderate vacuum after coating.

2.2.4. HRTEM Analysis. High-resolution transmission electron microscopy (HRTEM) analysis of copper catalyst was operated at 200 kV with a LIBRA 200FE analytical transmission electron microscope, equipped with FEG source and purchased from Zeiss. Samples were deposited on holey-carbon-coated grids from alcohol suspensions. Samples, in the form of powders, were ultrasonically dispersed in isopropyl alcohol, and a drop of the suspension was deposited on a holey-carbon film grid (300 mesh). Histograms of the particle size distribution (Figure S11) were obtained by counting onto the micrographs at least 500 particles; the mean particle diameter (d_m) was calculated by using the formula $d_m = \Sigma d_i n_i / \Sigma n_i$ where n_i was the number of particles of diameter d_i.

2.2.5. Surface Composition of the Catalysts — Cuboocta-hedron Model. Assuming that the catalyst nanoparticles are cubooctahedral in shape with a face-centered cubic (fcc) structure, it is possible to calculate the number of different sites depending on the size of the nanocrystals.[38,39] The total number of atoms of a copper nanoparticle for a fcc crystal (as is the case of copper) can be calculated from $d_{np} = 1.105 d_{at} N_T^{1/3}$, in which d_{np} is the average diameter of nanoparticles obtained by HRTEM and d_{at} is the atom diameter of copper (2.56 Å). The formula does not depend on particle shape.

Equation 1 allows one to calculate m, the length of an edge expressed as an atom.

$$N_T = (10m^3 - 15m^2 + 11^{m-3})/3 \tag{1}$$

All of the following, including N_B (bulk atoms), N_S (surface atoms), N_{HS} (high coordination atoms), and N_{LS} (low coordination atoms), are given from eqs 2−5:

$$N_B = 16m^3 - 63m^2 + 84m - 38 \tag{2}$$

$$N_S = 10m^2 - 20m + 12 \tag{3}$$

$$N_{HS} = 6(m - 2)^2 + 4(m - 3)(m - 2) \tag{4}$$

$$N_{LS} = 24(m - 2) + 12 \tag{5}$$

2.2.6. FT-IR Spectra of Adsorbed Probe Molecules (Pyridine and GVL). The FT-IR studies of probe molecules (pyridine and

presence of Ru supported on zeolitic or amorphous systems was put in evidence by Weckhuisen et al.[14] and by Fu et al.[30]

We have long been investigating the relationships between metal oxide dispersion and acidity in supported catalysts and recently reported on a new concept of solid Lewis catalyst.[31−33] Thus, we could show a relationship between the high dispersion of a non acidic oxide such as CuO and the acidic activity of a supported CuO/SiO₂ catalyst in epoxide ring opening, cellulose deconstruction, and Friedel Craft acylation.[34−36] Therefore, we were interested in investigating the acidity of the same system in the reduced state. If the acidity of the reduced Cu/SiO₂ catalyst was preserved, this would result in a true bifunctional catalyst where both acidic and reduction activity are carried out by the same site.

This may allow us to tune the activity and/or selectivity in the one-pot transformation of GVL into pentyl valerate by using a more simple catalyst.

Here we wish to report a detailed analysis of Cu/SiO₂ catalysts and catalytic tests showing that a more selective reaction can be obtained by using this bifunctional system where both the acidity and the hydrogenation activity can be ascribed to the metallic phase.

■ EXPERIMENTAL SECTION

2.1. Catalyst Preparation. Silica materials used as supports, SiO₂ A (SSA = 413 m²/g, PV = 0.75 mL/g) and SiO₂ B (SSA = 693 m²/g, PV = 0.62 mL/g), were obtained from Sigma-Aldrich and Sumitomo Chemicals, respectively.

Catalysts were prepared by the chemisorption−hydrolysis (CH) method[33] by adding the support to an aqueous $[Cu(NH_3)_4]^{2+}$ solution prepared by dropping NH_4OH to a $Cu(NO_3)_2 \cdot 3H_2O$ solution until pH 9 had been reached. After 20 min under stirring, the slurry, held in an ice bath at 0 °C, was diluted with water. The solid was separated by filtration with a Büchner funnel, washed with water, dried overnight at 120 °C, and calcined in air at 350 °C. Two series of catalysts were obtained with a nominal copper loading of 8% and 16%, respectively.

2.2. Catalyst Characterization. *2.2.1. Inductively Coupled Plasma (ICP) Analysis.* Copper metal loadings were determined by ICP-OES (ICAP6300 Duo purchased from Thermo Fisher Scientific) and an external calibration methodology, after microwave digestion of the samples (ca. 10 mg of catalyst, and therefore 0.8−1.5 mg of Cu) in 3 mL of aqua regia

Table 1. Morphological Data of the Samples Obtained from N$_2$ Adsorption−Desorption[a]

material	Cu content (%)	surface area (m$^2 \cdot$g^{-1})	PV (mL/g)	average pore diameter[b] (Å)
SiO$_2$ A		412.8	0.75	72
8% CuO/SiO$_2$ A	9.4	384.7	0.77	80
16% CuO/SiO$_2$ A	15.4	350.9	0.52	58
SiO$_2$ B		692.9	0.62	36
8% CuO/SiO$_2$ B	9.1	228.6	0.43	75
16% CuO/SiO$_2$ B	12.1	318.6	0.42	53

[a]See Figure S1. [b]Determined by the Gurvitsch rule.

GVL) adsorption and desorption were carried out with a FTS-60 spectrophotometer equipped with mid-IR MCT detector purchased from BioRad. The experiments were performed on sample disk (15−20 mg) after a simple calcination treatment (270 °C, 20 min air + 20 min under vacuum) for SiO$_2$ and CuO/SiO$_2$ samples or after a reduction pretreatment (270 °C, 20 min air + 20 min under vacuum + reduction under H$_2$) for Cu/SiO$_2$ samples. One spectrum was collected before probe molecule adsorption as a blank experiment. Therefore, pyridine (Py) or GVL adsorption was carried out at room temperature, and the following desorption steps were performed from room temperature to 250 °C. The spectrum of each desorption step was acquired every 50 °C after cooling the sample. IR spectra of adsorbed GVL were deconvoluted, by a peak fitting procedure, using GRAMS/AI software (Thermo Scientific Inc., U.S.A.).

2.2.7. Acidity Determination. Acidity measurements of the supports and catalysts have been performed in a home-assembled liquid chromatographic (HPLC) line, consisting of a L-6200A pump, an AS-2000A auto sampler injector, and a L-4250 UV−vis detector all purchased from Merck-Hitachi coupled to a personal computer for the collection, storage, and processing of the data.[40] The analyses have been performed by using 2-phenylethylamine (PEA) as probe molecule; PEA was dissolved in cyclohexane (for the intrinsic acidity) and in 1-pentanol (for the effective acidity) working at constant temperature of 30 ± 1 °C. The sample (ca. 0.050 g, 80−200 mesh particles) was first activated under air flowing (the calcined samples at 150 °C for 2 h) in a stainless steel tube (i.d. 2 mm, length 12 cm). After the transfer of the tube into the adsorption line, successive injections of PEA solution (50 μL, 0.15 M in cyclohexane or 1-pentanol) were put into the line in which the basic solution continuously circulated through the sample holder, until adsorption equilibrium was achieved. During the first run, the injections of PEA solution (50 μL) were done until surface saturation; then pure liquid was flowed (250 mL) through the sample to remove the physisorbed PEA, and the second run adsorption was collected. Subtraction of the second run from the first gives the chemisorption isotherm, from which the strong acid sites can be computed.

2.2.8. Temperature-Programmed Reductions. Temperature-programmed reduction (TPR) analysis was performed with a modified version of the Pulse Chemisorb 2700 apparatus from Micromeritics. Catalysts (samples containing ca. 2 mg of Cu) were diluted with quartz, calcined at 500 °C under O$_2$ (40 mL/min), and then reduced at 8 °C/min under a flow (15 mL/min) of a 8% H$_2$/Ar mixture. The H$_2$ consumption was detected by a thermal conductivity detector (TCD).

2.3. General Procedure for the Synthesis of Alkyl Valerates. In a typical run, the procedure which we followed is as follows: GVL (99% from Sigma-Aldrich, 4 g, 40 mmol), 1-pentanol (200 mmol) and catalyst (400 mg) were loaded in a Parr reactor under 10 atm H$_2$ at 250 °C for 10 h. The catalyst

was prereduced at 270 °C (20 min in air + 20 min under vacuum + reduction under H$_2$). The reaction mixture was analyzed by GC-MS (GC-MS chromatography, 5%-phenyl-methyl polysiloxane column) with the following temperature programm (60 °C for 3 min; 2,5 °C/min until 90 °C, 15 °C/min until 280 °C, 12 min at 280 °C) and by verifying the linear response in a concentration range of 0.01−0.1 M.

■ RESULTS AND DISCUSSION

The textural features of the two series of materials show a different behavior (See Table 1 and Figure 1). On silica A, we
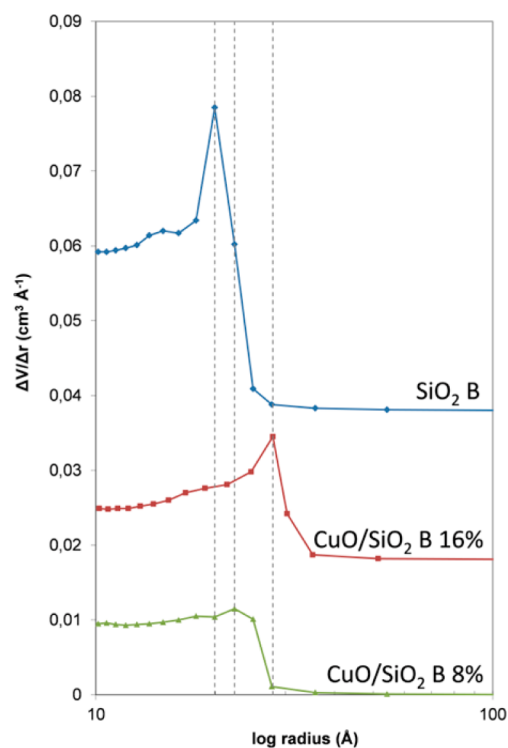

Figure 1. Pore volume distribution as a function of pore radius for support (SiO$_2$ B) and Cu catalysts (see Figure S2 for SiO$_2$ A).

observed a small decrease of the surface area going from the support to the 8% Cu catalyst and to the 16% Cu catalyst, whereas on silica B, we observed a dramatic decrease in the surface area values going from the support to the 8% Cu catalyst and then an increase going to the 16% Cu material. This second behavior can be explained by a very high dispersion on the support of the CuO phase in the 8% sample, covering two-thirds of the surface and filling the smallest pores, as shown by a decrease in pore volume and an increase in pore radius. When the Cu loading was increased to 16%, the CuO

particles grow outside the pores developing a new surface and causing the increase in surface area.

The behavior discussed above concerning the material microstructure is also consistent with the SEM images collected on the silica support and the copper catalysts. In particular, Figure S3 in the Supporting Information section shows the comparison between the smooth polyhedral grains of silica B and the wrinkled surface of the relevant highest copper catalyst, whose silica grains are covered by a new phase grown on it.

In spite of this evidence, TPR profiles of all the catalytic systems analyzed show a single and sharp reduction peak with the maximum centered around 250 °C (Figure 2). These data demonstrate that although the metal loading is quite high, the very high dispersion of the copper oxide phase allows its easy reduction to the metallic state.
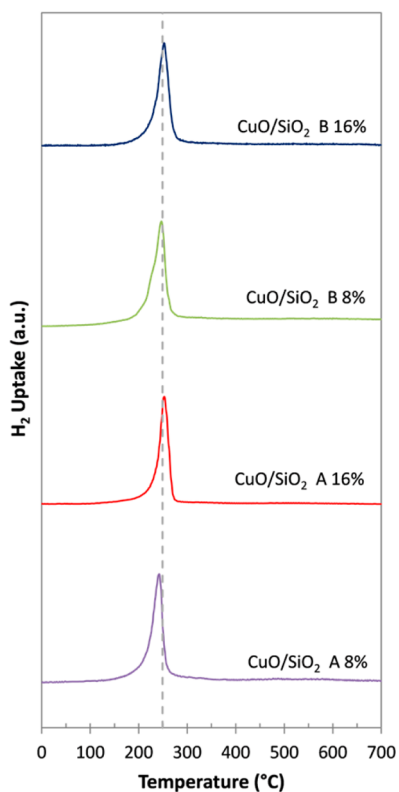

Figure 2. TPR reduction profiles for CuO/SiO$_2$ A (8% and 16% Cu) and CuO/SiO$_2$ B (8% and 16% Cu).

Some of us recently reported that copper catalysts supported on non acidic silica show acidic properties because of the high dispersion obtained with the preparation method, namely, the CH one.[33] Thus, pyridine desorption spectra of the fresh catalyst CuO/SiO$_2$ prepared by CH were compared with the spectrum of the bare SiO$_2$ support, and this comparison provides evidence for the presence of Lewis acid sites on the CuO containing material.

On the other hand, the very great advantage offered by a dispersed metal-containing phase would be the opportunity to also exploit other properties of the metal such as hydrogenation activity,[41] providing that the reduced phase preserve the acidic properties. In the present paper, we therefore compared the prereduced Cu/SiO$_2$ material with its parent CuO/SiO$_2$ in order to investigate its character. Moreover, we moved to another silica support with similar pore volume and much

higher surface area in order to further increase the metallic phase dispersion.

In order to directly compare the acidity of supported Cu systems, we used Py adsorption spectroscopy. Pyridine is a common basic probe molecule used to investigate the surface acidity of solid materials and gives also the chance to distinguish between Lewis and Brønsted acid sites.

FT-IR spectra of adsorbed pyridine are known to show many peaks ranging from 1400 to 1700 cm^{-1}. Pyridine bound to Lewis acid sites (L) is usually assigned to a first band around 1450 cm^{-1} and a second around 1610 cm^{-1}, whereas an absorption at 1550 cm^{-1} followed by a peak near 1640 cm^{-1} is related to the presence of Brønsted acid sites (Br). On the other hand, the band at around 1490 cm^{-1} is not clearly assigned and should be the result of a combination of pyridine lying on both Lewis and Brønsted acid sites, whereas a band at 1620 cm^{-1} was identified as the result of either kind of interactions. Finally, a weak interaction between the pyridine and the solid surface (physisorption or hydrogen bonding, P), resulting from very weak or no acidity, accounts for a two bands in the region of 1440−1450 cm^{-1} and at 1580−1600 cm^{-1}, which almost completely disappear by outgassing at 100 °C.[35,42−45]

The analyzed catalysts, both reduced and unreduced ones, show the presence of the bands ascribable to Lewis acid sites at 1450 and 1610 cm^{-1} that are resistant to the outgassing at high temperatures, at least up to 250 °C, whereas physisorbed pyridine completely disappears at 100 °C (Figure 3, S5−S10). On the other hand, spectra of both silica supports show only the two bands of physisorbed pyridine.

From the spectra here reported, it is evident that the reduced samples exposing metallic copper on the surface not only keep the properties of the precursor CuO phase (the same bands in the spectra are even more evident) but also show an even increased Lewis acid character with respect to the unreduced materials.

Thus, the amount of adsorbed pyridine (mmol$_{Py}$/g$_{cat}$), calculated on the basis of the relationship reported by Emeis[46] from the integration of the band around 1450 cm^{-1}, clearly show this trend, both in the case of Cu/SiO$_2$ A and of Cu/SiO$_2$ B (see Table 2). This amplification results to be almost 5 times in the case of Cu/SiO$_2$ B versus CuO/SiO$_2$ B (0.342 mmol$_{Py}$/g$_{cat}$ vs 0.073 mmol$_{Py}$/g$_{cat}$).

Moreover, in the spectra of adsorbed pyridine on reduced copper catalysts, also a significant band at 1575 cm^{-1} and a shoulder at 1441 cm^{-1}, respectively, are visible. These two bands are ascribable to the 8b and 19b modes of adsorbed pyridine[47] corresponding to the vibrational modes as those of benzene ring.[48] The presence of these bands is therefore even more diagnostic of the Lewis-type interaction of these catalytic systems with pyridine (Figure 3).

To have a deeper insight into the acidic properties of Cu/SiO$_2$ B, liquid-phase acid−base titrations by a strong base probe, 2-phenylethylamine (PEA) was also performed. For the titrations, cyclohexane was chosen to dissolve PEA. As a result of the apolar aprotic character of cyclohexane, the amount of the acid sites determined in this liquid corresponds to the *intrinsic* acidity of the samples.[40,45]

Figure 4 shows the PEA adsorption isotherms of silica B and of the two copper catalysts at different loadings collected in cyclohexane. All the isotherms, both those related to the first adsorption run and those of the second adsorption run, have a more or less Langmuirian shape. The computed chemisorption
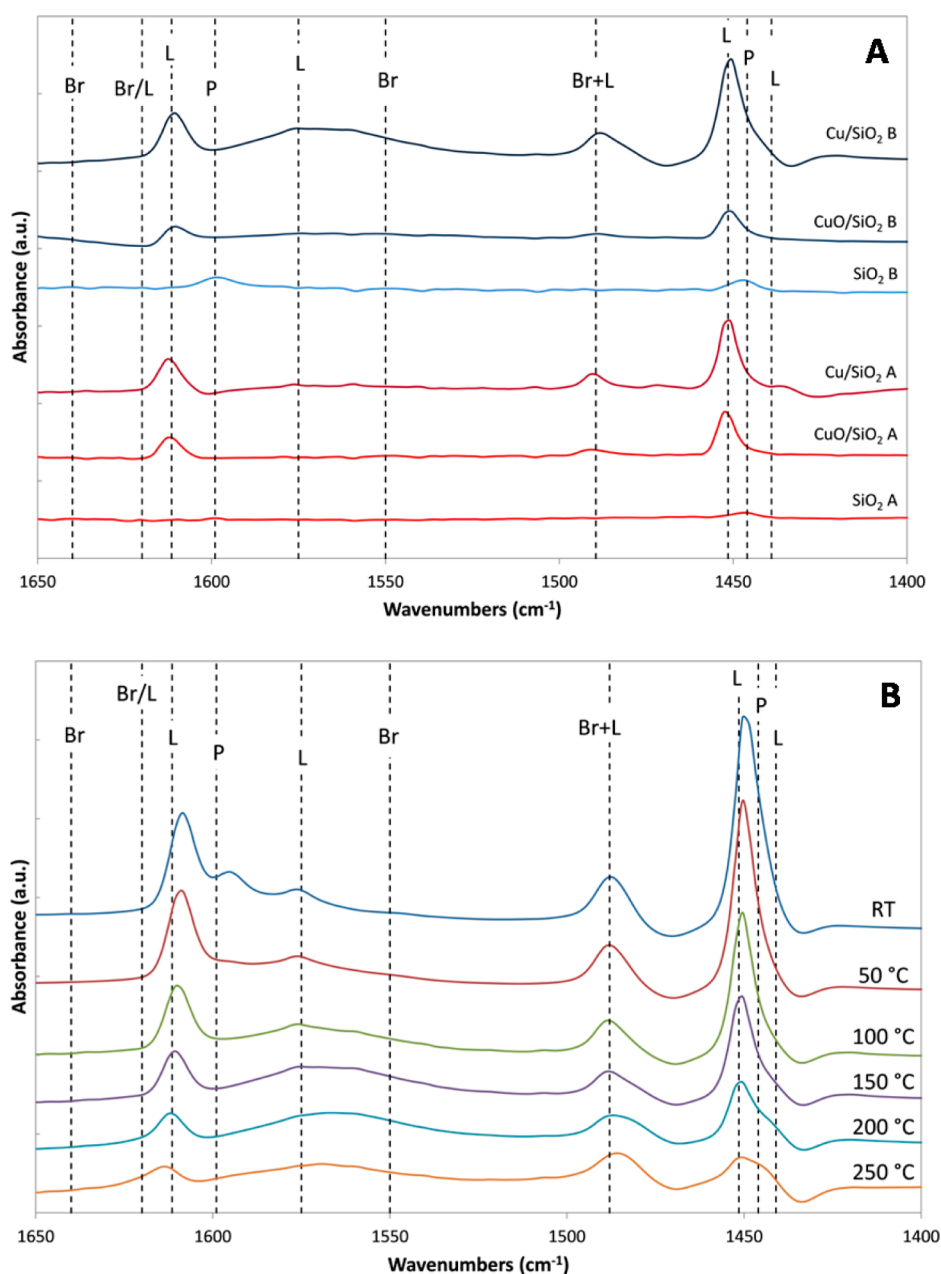
Figure 3. IR spectra of adsorbed pyridine on different catalysts. (A) Comparison of bare silicas (SiO₂ A and SiO₂ B), unreduced copper supported catalysts (16% CuO/SiO₂ A and 16% CuO/SiO₂ B), and reduced ones (16% Cu/SiO₂ A and 16% Cu/SiO₂ B) after adsorption of Py and degassing at 150 °C. (B) Py adsorption patterns at different desorption temperature for 16% Cu/SiO₂ B.

Table 2. Amount of Adsorbed Pyridine ($mmol_{Py}/g_{cat}$) on the Different Catalysts (Reduced and Not Reduced) Evaluated from the Band at 1450 cm⁻¹

	pyridine on L sites (mmol/g)		
sample	150 °C	200 °C	250 °C
16% CuO/SiO₂ A	0.096	0.067	0.047
16% Cu/SiO₂A	0.156	0.121	0.089
16% CuO/SiO₂ B	0.073	0.049	0.036
16% Cu/SiO₂ B	0.342	0.240	0.159
8% Cu/SiO₂ B	0.236	0.155	0.101

isotherms, related to the strong acid sites of the samples, have a more pronounced Langmuirian shape, as expected.

Results obtained from the titrations have been collected in Table 3. It can be observed that silica shows the highest amount of total acid sites and of strong acid sites (expressed in terms of equivalent of sites per unit mass, m_{eq}/g) among the samples because of its higher surface area. The percentage of strong acidic sites increases from silica (52%) to the 8% Cu sample (60%) and the 16% Cu sample (71%); then, concerning the acid strength, the following ranking can be observed: 16% Cu/SiO₂ B > 8% Cu/SiO₂ B > SiO₂ B (Table 3). This clearly shows the change in the nature of acidic sites going from silica to the Cu catalysts, which are also associated with Lewis Cu centers.

The Lewis acidity expressed by CuO/SiO₂ is quite unusual as CuO in its bulk form shows, on the contrary, a basic behavior. This character was previously ascribed to the surface defectivity of the highly dispersed CuO phase, shown to be in distorted
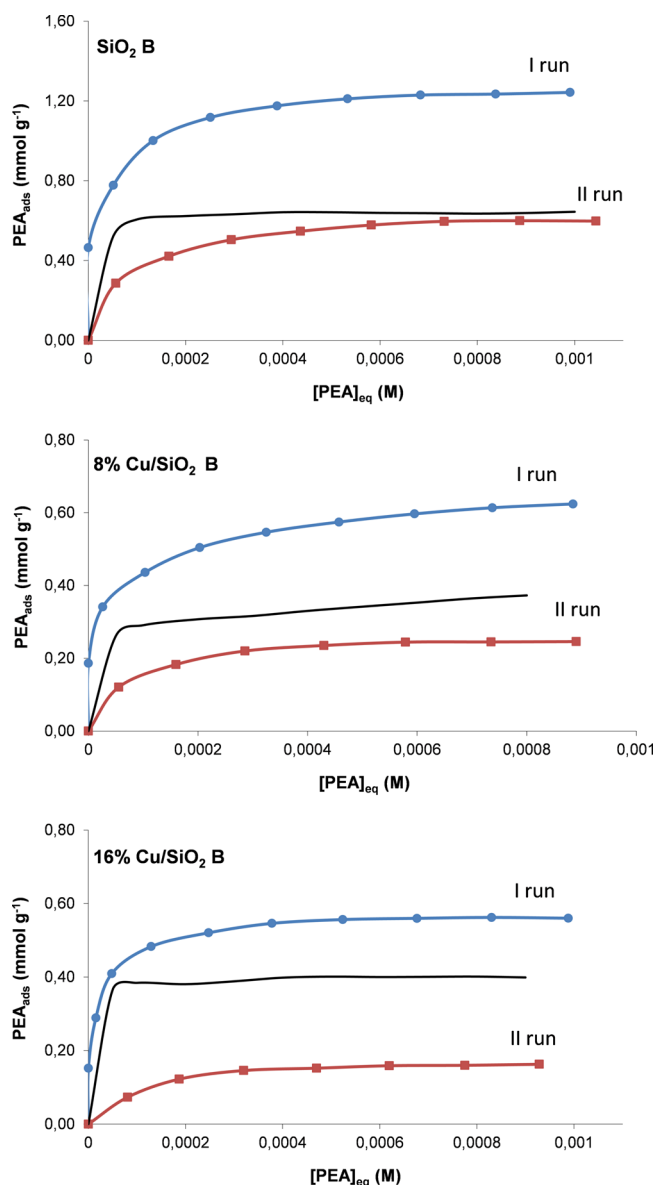
Figure 4. First (blue full circle line) and second (red full square line) runs of PEA adsorption isotherms collected at 30 °C in cyclohexane on SiO$_2$ B and relevant Cu catalysts; the chemisorption isotherm (black solid line) has been computed from subtraction of the second from the first isotherm.

Table 3. Results of the *Intrinsic* Acidity Determination Collected in Cyclohexane

code	*intrinsic* acid sites	
	total	strong
	mmol·g^{-1}	
SiO$_2$ B	1.236	0.641 (52%)
8% Cu/SiO$_2$ B	0.627	0.376 (60%)
16% Cu/SiO$_2$ B	0.561	0.400 (71%)

octahedral configuration by means of EXAFS and DRUV spectroscopic analysis,[33] that is a peculiarity deriving from the CH preparation technique. The reduction of copper oxide into Cu(0) enhances even more this defectivity, the cuboctahedron or truncated octahedron being the best approximations for the geometry of a metallic nanoparticle[39,49] thus resulting in a

higher concentration of Lewis sites. To get a deeper insight into the dispersion and morphology of the Cu metallic phase high resolution micrographs of the 16% Cu/SiO$_2$ B sample were recorded. The lattice-fringe image/FFT of a representative Cu particle on the surface (Figure 5B,C) shows spots at 2.1 and 1.8
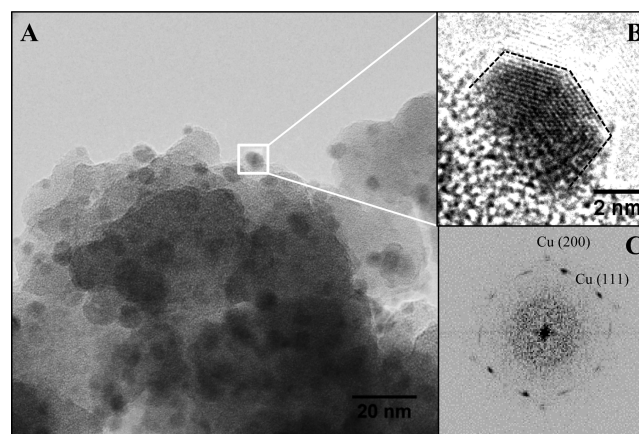

Figure 5. (A) HRTEM micrographs of 16% Cu/SiO$_2$ B catalyst; (B) magnified view of the Cu nanoparticle squared in A; (C) inverted FFT pattern taken from image B.

Å, corresponding to Cu (111) and Cu (200) lattice planes of metallic copper, respectively. High resolution micrographs together with the observed spots in the FT pattern are in good agreement with the presence of cuboctahedron copper particles in a face cubic centered (fcc) crystal structure.[50,51] Moreover, transmission electron micrographs (Figure 5A) show well-dispersed spherical Cu nanoparticles over the SiO$_2$ support with particle size centered at about 4.7 nm (Figure S11). Therefore, HRTEM analysis clearly shows the presence of well dispersed metallic phase with well formed, highly defective metal nanoparticle.

These findings prompted us to test the activity of these materials in the one-pot conversion of GVL into pentyl valerate (PV) (Scheme 1). Previous results obtained in the same transformation with Cu/SiO$_2$–ZrO$_2$ clearly showed the importance of both acidic and hydrogenation activity for this transformation.[27] The use of an acidic mixed oxide such as silica zirconia as the support granted the presence of acidic sites, whereas the well-dispersed, reduced copper phase allowed the reduction of alkyl pentenoates into alkyl valerates.

We therefore found it compelling to investigate whether the catalyst presenting the higher density of Lewis sites, namely, 16% Cu/SiO$_2$ B, was able to behave as a true polyfunctional catalyst, where nucleophilic addition to the carbonyl group, dehydration of the intermediate alcohol **1**, and hydrogenation of pentenoate **2** are all promoted by the metallic phase.

Table 4 reports turnover frequencies calculated after a 1 h reaction for 8% Cu/SiO$_2$–ZrO$_2$ and 16% Cu/SiO$_2$ catalysts with respect to total surface atoms, high coordination sites, and low coordination sites according to a cuboctrahedron model, as well as Lewis sites as evaluated from pyridine adsorption spectra. The ratio between the two values calculated for low coordination sites and for Lewis sites are close to 1, clearly showing that Lewis behavior is linked with low coordination sites on the metal particle.

Further insights into the role of copper can be drawn by analyzing the IR spectra of adsorbed GVL (see Figure 6). The spectrum of GVL adsorbed onto SiO$_2$ B shows two bands, one

Table 4. Turnover Frequencies Evaluated after a 1 h reaction and Calculated on Both Surface Atoms and Acidic Sites

| | D^a (nm) | L^b (mmol$_{Py}$/g$_{cat}$) | conv (%) | TOF^c (h^{-1}) | | | TOF^d (h^{-1}) |
				N_S	N_{HS}	N_{LS}	L
16% Cu/SiO$_2$ B	4.7	0.159	49	104.6	133.3	486.3	308.2
8% Cu/SiO$_2$–ZrO$_2$	3.7	0.183	54	125.3	172.3	459.5	295.4

^{a}Mean particle diameter evaluated by HRTEM. ^{b}Lewis acid sites density evaluated by adsorbed pyridine titration after degassing at 250 °C. ^{c}TOF (after 1 h reaction) evaluated by using the surface atoms composition according to the cuboctahedral shape model reported by Kaneda.[39] ^{d}TOF (after 1 h reaction) evaluated on Lewis acidic sites L.
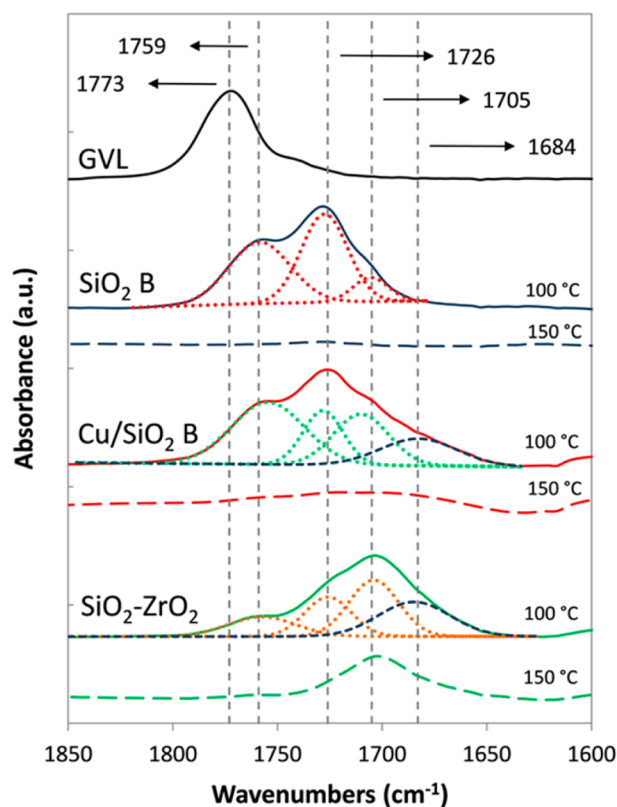

Figure 6. GVL adsorption IR spectra after outgassing at 150 and 100 °C for SiO$_2$ B, Cu/SiO$_2$ B, and SiO$_2$–ZrO$_2$ compared with the spectrum of pure GVL.

corresponding to the physisorbed molecule[52] centered at 1759 cm^{-1} and one at 1726 cm^{-1}, ascribable to a weak chemical interaction with GVL. This band is indeed still evident, although very weak, also after degassing at 150 °C, whereas the band at 1759 cm^{-1} completely disappears under these conditions. When Cu is present on the same SiO$_2$, a shoulder lying at wavenumber lower than 1700 cm^{-1} is also present witnessing a strong chemisorption of GVL C=O double bond with the catalyst.

Indeed, deconvolution of the spectrum shows that three bands are present in the case of GVL adsorbed on SiO$_2$ (1759, 1726, and 1705 cm^{-1}), whereas on Cu/SiO$_2$, a new band, centered at 1683 cm^{-1}, is clearly detectable.

It is interesting to note that this same signal at 1683 cm^{-1} is present also in the bare SiO$_2$–ZrO$_2$ spectrum (with a very small shift to 1685 cm^{-1}), showing a very similar behavior of the two materials, at least with respect to GVL.

These spectra strongly confirm the hypothesis of the relevant role of reduced copper not only in the hydrogenation reaction but also in the activation of the substrate toward nucleophilic addition by virtue of its Lewis acidic properties (Scheme 2). It

is worth noting that the interaction with silica catalysts is generally more labile with degassing at increasing temperature with respect to the one with silica zirconia.

Scheme 2. Schematic Representation of the GVL Ring Opening Reaction Mechanism Activated by the Cu/SiO$_2$ Catalyst
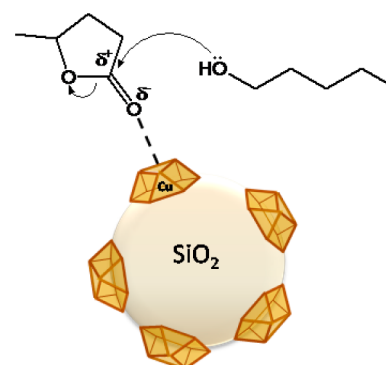
The presence of a unique catalytic site and in particular the absence of catalytically relevant Brønsted acid sites on the support may in fact have a positive effect on product selectivity. Results obtained in the catalytic tests for longer reaction times are reported in Table 5.

Table 5. Reaction of GVL with 1-Pentanol To Form Pentyl Valerate^a

entry	catalyst	conv (%)	Sel PV (%)	Sel 1 (%)	Sel 2 (%)	Sel 4 (%)
1	no catalyst	30		70		12
2	SiO$_2$ B	7		9	14	57
3	SiO$_2$–ZrO$_2$	58		1	51	40
4	8% Cu/SiO$_2$–ZrO$_2$	92	72			16
5	16% Cu/SiO$_2$ A	81	70	10		4
6	8% Cu/SiO$_2$ B	75	77	11		5
7	16% Cu/SiO$_2$ B	91	92			7
8	16% CuO/SiO$_2$ B^b	83	65	8		3

^{a}Reaction conditions: 0.1 wt % catalyst, 250 °C, 10 bar H$_2$, 690 rpm, 10h, GVL/pentanol = 1:5. ^{b}Unreduced catalyst.

These data agree well with pyridine characterization, the catalyst showing the highest number of Lewis acid sites, namely, the reduced 16% Cu/SiO$_2$ B being the most selective material. On the other hand, the unreduced 16% CuO/SiO$_2$ B, the reduced 8% Cu/SiO$_2$ B, and catalysts prepared on SiO$_2$ A are less active.

The use of naked silica as a catalyst, even with very low conversion, gave selectively product **4** coming from dehydration between the intermediate hydroxyl compound **1** and the solvent alcohol, which is also favored on the naked silica

zirconia catalyst (entry 3), suggesting a determining role of Bronsted-like sites in this pathway.

When Cu is deposited on the surface the decrease in this kind of acidic sites, witnessed by intrinsic acidity measurements carried out with PEA, results in a very low selectivity toward the ether in favor of the olefinic compound **2**, which is then hydrogenated to pentyl valerate (PV) and never accumulates in the reaction mixture. The high selectivity observed (entry 7) is therefore due to both the contribution to acidity of the metallic phase and its high hydrogenation activity, thereby driving the reaction toward the upper reaction pathway (Scheme 1). This effect is even more pronounced in the case of copper deposited on SiO_2 with respect to Cu/SiO_2-ZrO_2, because residual Bronsted-like sites on the surface of silica-zirconia make the lower pathway still possible.

This is in agreement with the very low number of acid sites observed when titrating with PEA dissolved in 1-pentanol (i.e., the actual reaction solvent). The acidity determined in 1-pentanol corresponds to the *effective* acidity shown by the sample surface in the reaction liquid.[53] Acid−base titration analysis carried out in the same or similar reaction solvent allows one to evaluate acidity under conditions similar to those used during reaction. The amount of *effective* sites is relevant for silica and increases in the presence of the supported metal.

All these observations are consistent with the reaction mechanisms proposed. Thus, the reaction of GVL in the presence of strong Bronsted sites such as those present on the surface of Ru/H-β and Ru/H-ZSM5 or Ru/SBA-SO₃H gives pentenoic and pentanoic acids[14,30] that are then esterified. On the contrary, in the presence of Cu/SiO_2, the lactone ring is opened by nucleophilic attack of 1-pentanol to the carbonyl group activated through interaction with the Lewis acid sites on the catalyst surface.

CONCLUSIONS

The role of metal dispersion in determining the catalytic activity in hydrogenation and oxidation reactions has long been recognized. On the contrary, the influence of the supported metal particle size on the acidic properties of the catalyst has very rarely been investigated. The present paper shows that very small metal particles can exhibit catalytically relevant Lewis acidity. This property, joined with a significant hydrogenation activity of the metal, allows one to design new bifunctional catalysts, such as Cu/SiO_2, without the need of an acidic support. In the case of GVL to pentyl valerate reaction, this translates not only into a more simple catalytic system but also into a more selective one as a result of the presence of a unique catalytic site that prevents secondary reactions to take place.

ASSOCIATED CONTENT

Ⓢ Supporting Information

N_2 adsorption/desorption isotherms; pore volume distribution as a function of pore radius for SiO_2 A and Cu/SiO_2 A; SEM images of silica B surface and 16% Cu catalyst surfaces; XRD of 16% CuO/SiO_2 B; py adsorption spectra at different desorption temperature for all reduced and unreduced Cu catalysts; HRTEM micrograph and particle size distribution of 16% Cu/SiO_2 B catalyst. This material is available free of charge via the Internet at http://pubs.acs.org.

AUTHOR INFORMATION

Corresponding Author

*E-mail: n.ravasio@istm.cnr.it. Fax: +39 0250314405. Tel.: +39 0250314382.

Author Contributions

§N.S. and M.D. contributed equally.

Notes

The authors declare no competing financial interest.

REFERENCES

(1) Perego, C.; Ricci, M. *Catal. Sci. Technol.* **2012**, *2*, 1776−1786.

(2) Bozell, J. J. *Green Chem.* **2010**, *12*, 525−728.

(3) Climent, M. J.; Corma, A.; Iborra, S. *Green Chem.* **2014**, *16*, 516−547.

(4) Bermudez, J. M.; Menéndez, J. A.; Romero, A. A.; Serrano, E.; Garcia-Martinez, J.; Luque, R. *Green Chem.* **2013**, *15*, 2786−2792.

(5) Upare, P. P.; Lee, J.-M.; Hwang, Y. K.; Hwang, D. W.; Lee, J.-H.; Shiva, B.; Halligudi, S. B.; Hwang, J.-S.; Chang, J.-S. *ChemSusChem* **2011**, *4*, 1749−1752.

(6) Yang, Y.; Gao, G.; Zhang, X.; Li, F. *ACS Catal.* **2014**, *4*, 1419−1425.

(7) Yan, K.; Lafleur, T.; Jarvis, C.; Wu, G. *J. Cleaner Prod.* **2014**, *72*, 230−232.

(8) Abdelrahman, O. A.; Heyden, A.; Bond, J. Q. *ACS Catal.* **2014**, *4*, 1171−1181.

(9) Mohan, V.; Venkateshwarlu, V.; Pramod, C. V.; Raju, B. D.; Rao, K. S. R. *Catal. Sci. Technol.* **2014**, *4*, 1253−1259.

(10) Fabos, V.; Mika, L. T.; Horvath, I. T. *Organometallics* **2014**, *33*, 181−187.

(11) Tang, X.; Chen, H.; Hu, L.; Hao, W.; Sun, Y.; Zeng, X.; Lin, L.; Liu, S. *Appl. Catal., B* **2014**, *147*, 827−834.

(12) Yang, Z.; Huang, Y.-B.; Guo, Q.-X.; Fu, Y. *Chem. Commun.* **2013**, *49*, 5328−5330.

(13) Yuan, J.; Li, S.-S.; Yu, L.; Liu, Y.-M.; Cao, Y.; He, H.-Y.; Fan, K.-N. *Energy Environ. Sci.* **2013**, *6*, 3308−3313.

(14) Luo, W.; Upakul Deka, U.; Andrew, M.; Beale, A. M.; Ernst, R. H.; van Eck, E. R. H.; Pieter, C. A.; Bruijnincx, P. C. A.; Weckhuysen, B. M. *J. Catal.* **2013**, *301*, 175−186.

(15) Horvath, I. T.; Mehdi, H.; Fabos, V.; Boda, L.; Mika, L. T. *Green Chem.* **2008**, *10*, 238−242.

(16) Fegyverneki, D.; Orha, L.; Lang, G.; Horvath, I. T. *Tetrahedron* **2010**, *66*, 1078−1081.

(17) Luterbacher, J. S.; Rand, J. M.; Martin Alonso, D.; Han, J.; Tyler Youngquist, J.; Maravelias, C. T.; Pfleger, B. F.; Dumesic, J. A. *Science* **2014**, *343*, 277−280.

(18) Qi, L.; Fung Mui, Y.; Wing Lo, S.; Lui, M. Y.; Akien, G. R.; Horvath, I. T. *ACS Catal.* **2014**, *4*, 1470−1477.

(19) Martin Alonso, D.; Wettstein, S. G.; Dumesic, J. A. *Green Chem.* **2013**, *15*, 584−595.

(20) Serrano-Ruiz, J. C.; Luque, R.; Sepulveda-Escribano, A. *Chem. Soc. Rev.* **2011**, *40*, 5266−5281.

(21) Martin Alonso, D.; Wettstein, S. G.; Bond, J. Q.; Root, T. W.; Dumesic, J. A. *ChemSusChem* **2011**, *4*, 1078−1081.

(22) Bond, J. Q.; Martin Alonso, D.; Wang, D.; West, R. M.; Dumesic, J. A. *Science* **2010**, *327*, 1110−1114.

(23) Bozell, J. J. *Science* **2010**, *329*, 522−523.

(24) Serrano-Ruiz, J. C.; Braden, D. J.; West, R. M.; Dumesic, J. A. *Appl. Catal., B* **2010**, *100*, 184−189.

(25) Bond, J. Q.; Martin Alonso, D.; West, R. M.; Dumesic, J. A. *Langmuir* **2010**, *26*, 16291−16298.

(26) Lange, J.-P.; Price, R.; Ayoub, P. M.; Louis, J.; Petrus, L.; Clarke, L.; Gosselink, H. *Angew. Chem., Int. Ed.* **2010**, *49*, 4479−4483.

(27) Chan-Thaw, C. E.; Marelli, M.; Psaro, R.; Ravasio, N.; Zaccheria, F. *RSC Adv.* **2013**, *3*, 1302−1306.

(28) Shimizu, K.; Satsuma, A. *Energy Environ. Sci.* **2011**, *4*, 3140−3153.

(29) Shimizu, K.; Furukawa, H.; Kobayashi, N.; Itaya, Y.; Satsuma, A. *Green Chem.* **2009**, *11*, 1627−1632.

(30) Pan, T.; Deng, J.; Xu, Q.; Xu, Y.; Guo, Q.-X.; Fu, Y. *Green Chem.* **2013**, *15*, 2967−2974.

(31) Gervasini, A.; Messi, C.; Ponti, A.; Cenedese, S.; Ravasio, N. *J. Phys. Chem. C* **2008**, *112*, 4635−4642.

(32) Ravasio, N.; Zaccheria, F.; Gervasini, A.; Messi, C. *Catal. Commun.* **2008**, *9*, 1125−1127.

(33) Zaccheria, F.; Scotti, N.; Marelli, M.; Psaro, R.; Ravasio, N. *Dalton Trans.* **2013**, *42*, 1319−1327.

(34) Zaccheria, F.; Santoro, F.; Psaro, R.; Ravasio, N. *Green Chem.* **2011**, *13*, 545−548.

(35) Mariani, M.; Zaccheria, F.; Psaro, R.; Ravasio, N. *Catal. Commun.* **2014**, *44*, 19−23.

(36) Zaccheria, F.; Shaikh, N. I.; Scotti, N.; Psaro, R.; Ravasio, N. *Top. Catal.* **2014**, *57*, 1085−1093.

(37) Barrett, E. P.; Joyner, L. G.; Halenda, P. P. *J. Am. Chem. Soc.* **1951**, *73*, 373−380.

(38) Benfield, R. E. *J. Chem. Soc., Faraday Trans.* **1992**, *88*, 1107.

(39) Mori, K.; Hara, T.; Mizugaki, T.; Ebitani, K.; Kaneda, K. *J. Am. Chem. Soc.* **2004**, *126*, 10657−10666.

(40) Carniti, P.; Gervasini, A.; Marzo, M. *Catal. Today* **2010**, *152*, 42−47.

(41) Zaccheria, F.; Psaro, R.; Ravasio, N. *Green Chem.* **2009**, *11*, 462−465.

(42) Hensen, E. J. M.; Poduval, D. G.; Degirmenci, V.; Michel Ligthart, D. A. J.; Chen, W. F.; Maugé, F.; Rigutto, M. S.; van Veen, J. A. R. *J. Phys. Chem. C* **2012**, *116*, 21416−21429.

(43) Parry, E. P. *J. Catal.* **1963**, *2*, 371−379.

(44) Busca, G.; Martra, G.; Zecchina, A. *Catal. Today* **2000**, *56*, 361−370.

(45) Gervasini, A.; Bennici, S.; Auroux, A.; Guimon, C. *Appl. Catal., A* **2007**, *331*, 129−137.

(46) Emeis, C. A. *J. Catal.* **1993**, *141*, 347−354.

(47) Sánchez Escribano, G. V.; del Hoyo Martínez, C.; Fernández López, E.; Gallardo Amores, J. M.; Busca, G. *Catal. Commun.* **2009**, *10*, 861−864.

(48) Kumar, M.; Srivastava, M.; Yadav, R. A. *Spectrochim. Acta, Part A* **2013**, *111*, 242−251.

(49) Zhang, Q.; Deng, W.; Wang, Y. *Chem. Commun.* **2011**, *47*, 9275−9292.

(50) J. Urban, J.; H. Sack-Kongehl, H.; K.Weiss, K. *Catal. Lett.* **1997**, *49*, 101−108.

(51) Lignier, P.; Bellabarba, R.; Tooze, R. P. *Chem. Soc. Rev.* **2012**, *41*, 1708−1720.

(52) Tukacs, J. M.; Király, D.; Strádi, A.; Novodarszki, G.; Eke, Z.; Dibó, G.; Kégl, T.; Mika, L. T. *Green Chem.* **2012**, *14*, 2057−2065.

(53) Carniti, P.; Gervasini, A.; Biella, S.; Auroux, A. *Chem. Mater.* **2005**, *17*, 6128−6136.